ACS APPLIED MATERIALS & INTERFACES

Research Article

Cite This: ACS Appl. Mater. Interfaces 2019, 11, 3024−3033

www.acsami.org

Alkali Postdeposition Treatment-Induced Changes of the Chemical and Electronic Structure of Cu(In,Ga)Se_2 Thin-Film Solar Cell Absorbers: A First-Principle Perspective

Maria Malitckaya,[†] Thomas Kunze,[‡] Hannu-Pekka Komsa,[†] Ville Havu,[†] Evelyn Handick,[‡] Regan G. Wilks,[‡,§] Marcus Bär,[‡,§,∥,⊥] and Martti J. Puska*[,†]

[†]Department of Applied Physics, Aalto University, P.O. Box 11000, 00076 Aalto, Finland

[‡]Department of Interface Design and [§]Energy Materials In-Situ Laboratory Berlin (EMIL), Helmholtz-Zentrum Berlin für Materialien und Energie GmbH (HZB), 12489 Berlin, Germany

[∥]Helmholtz-Institute Erlangen-Nürnberg for Renewable Energy (HIERN), Forschungszentrum Jülich, 90429 Erlangen, Germany

[⊥]Department of Chemistry and Pharmacy, Friedrich-Alexander-Universität Erlangen-Nürnberg, 91054 Erlangen, Germany

Supporting Information

ABSTRACT: The effects of alkali postdeposition treatment (PDT) on the valence band structure of Cu(In,Ga)Se_2 (CIGSe) thin-film solar cell absorbers are addressed from a first-principles perspective. In detail, experimentally derived hard X-ray photoelectron spectroscopy (HAXPES) data [Handick, E.; et al. *ACS Appl. Mater. Interfaces* **2015**, *7*, 27414−27420] of the valence band structure of alkali-free and NaF/KF-PDT CIGSe are directly compared and fit by calculated density of states (DOS) of $CuInSe_2$, its Cu-deficient counterpart $CuIn_5Se_8$, and different potentially formed secondary phases, such as $KInSe_2$, InSe, and In_2Se_3. The DOSs are based on first-principles electronic structure calculations and weighted according to element-, symmetry-, and energy-dependent photoionization cross sections for the comparison to experimental data. The HAXPES spectra were recorded using photon energies ranging from 2 to 8 keV, allowing extraction of information from different sample depths. The analysis of the alkali-free CIGSe valence band structure reveals that it can best be described by a mixture of the DOS of $CuInSe_2$ and $CuIn_5Se_8$, resulting in a stoichiometry slightly more Cu-rich than that of $CuIn_3Se_5$. The NaF/KF-PDT-induced changes in the HAXPES spectra for different alkali exposures are best reproduced by additional contributions from $KInSe_2$, with some indications that the formation of a pronounced K−In−Se-type surface species might crucially depend on the amount of K available during PDT.

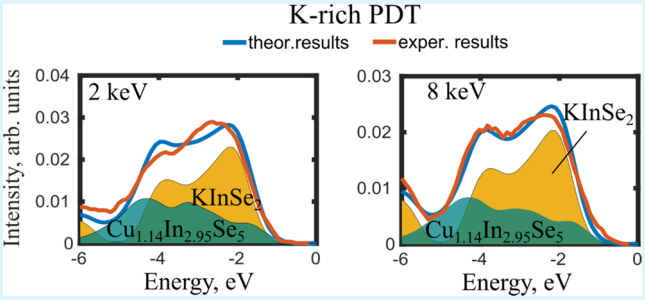

KEYWORDS: *chalcopyrite thin-film solar cells, KF-PDT, $KInSe_2$, DFT, HAXPES*

1. INTRODUCTION

The efficiency of Cu(In,Ga)Se_2 (CIGSe) solar cells increased relatively slowly during the first decade of the 21st century.[1,2] A significant leap forward resulted from the development of alkali fluoride postdeposition treatments (PDTs) carried out after the three-stage laboratory manufacturing process of CIGSe absorbers.[3] Initially, PDT was designed to reproduce the beneficial effects[4] of alkalies for absorber layers deposited on alkali-free (flexible) substrates, which in the case of CIGSe coevaporated on the standard soda-lime glass substrates inherently appearing via in-diffusion from the substrate.[4−6] Later, the efficiency improvements due to NaF- and KF-PDT were confirmed also for CIGSe absorbers grown on soda-lime glasses[7] or steel substrates.[8] Recently, even higher efficiencies were obtained by using heavier alkali elements, like Rb (22.6%[9]) and Cs (22.9%[10]), in optimized PDT processes.

The effects of light alkalies on the properties of CIGSe absorbers and related solar cells have been studied extensively over the years.[3−9] According to several experiments, NaF-PDT results in improved open circuit voltage (V_{OC}) and fill factor (FF). Upon (additional) KF-PDT, even higher V_{OC} and FF were achieved. Moreover, employing a KF-PDT allows the deposition of thinner CdS buffer layers, which leads to reduced optical losses in the buffer, resulting in increased short circuit currents.[3−5,7] The KF-PDT-induced changes in surface composition (mainly Cu and Ga depletion and presence of K but not F) and surface morphology[3,11−16] have been associated with the formation of a K-containing surface species.[3,5,13−17] To correlate this secondary phase formation

Received: October 18, 2018
Accepted: December 28, 2018
Published: December 28, 2018

DOI: 10.1021/acsami.8b18216
ACS Appl. Mater. Interfaces 2019, 11, 3024−3033

at the absorber surface with changes in the electronic structure of the CIGSe absorber layer after KF-PDT, direct and inverse photoemission measurements have been used in previous studies.[14,17] The main finding has been that the KF-PDT process induces shifts of the valence band maximum (VBM) and the conduction band minimum away from the Fermi level, manifesting itself in a widening of the band gap at the absorber surface.[14,17] According to previous studies,[13,17] the VBM lowering cannot only be explained by a decrease in p−d interband repulsion related to the degree of Cu deficiency[18] but is also rather indicative of the formation of a K−In−Se-type surface species. The measured surface band gap of 2.5 eV[17] is consistent with the theoretical value for the secondary phase compound $KInSe_2$.[19,20]

Due to hybridization of the electronic states that form the valence band, a detailed analysis of respective photoelectron spectroscopy spectra can be challenging, in particular, if the spectra of the constituent phases are not known a priori. Here, we provide the missing information by means of first-principles simulations, which we use to model the experimental spectra published in refs 17, 21 (see Figure S1, Supporting Information (SI) for convenience). Briefly, we consider hard X-ray photoelectron spectra (HAXPES) data of the valence band region for three CIGSe samples (alkali-free, K-poor, and K-rich) measured with excitation energies of 2, 6, and 8 keV. The latter two samples were prepared employing a combined NaF/KF-PDT with a higher KF deposition rate for the last sample (for more details, see refs 3, 13, 17). The data of the alkali-free and K-rich CIGSe samples clearly show distinct changes in the spectral shape (see Figure S1), with the spectra of the K-poor CIGSe most likely being a linear combination (with relative shifts) of the first two data sets. Note that the employed excitation energies also influence the spectral shape due to changes in relative photoionization cross sections of the states forming the valence band as well as by a different probing depth (if the composition changes throughout the probed volume, which is defined by the exponential attenuation of the photoelectron signal within the sample). For photoelectrons from the valence band region, the kinetic energy increases similar to the excitation energy from 2, over 6, to 8 keV, resulting in an inelastic mean free path (IMFP) increase from 4, over 10, to 12 nm, respectively, for the valence band regime.[13,22]

In this work, we develop first-principles models that aim to reduce the measured HAXPES valence band spectra of the CIGSe absorber (surface) for which no PDT (i.e., alkali-free) or NaF/KF-PDT was performed as part of the preparation process. The ultimate goal is to reveal the chemical and electronic absorber structure and how it is impacted by alkali PDT. Of particular relevance would be any insight into whether or not a K−In−Se-type species is formed on top of the NaF/KF-PDT CIGSe absorber even in cases where the absorber is treated with moderate or low amounts of K. To do so, we derive simulated HAXPES valence band spectra by using first-principles density functional theory (DFT) electronic structures of crystalline Cu−In−Se phases with different compositions as well as those of potentially formed (K−)In−Se secondary phases. We omit Ga in our simulations, because it is depleted at KF-PDT CIGSe surfaces.[3,13] We assume that the absorber surface could consist of six possible compounds: $CuInSe_2$, $CuIn_5Se_8$, $KInSe_2$ (having a monoclinic or chalcopyrite crystal structure[18]), InSe, and In_2Se_3. The computed crystal structures and lattice constants are given in Figure S2 and Table S1, respectively. Besides the ordered defect compound phase $CuIn_5Se_8$, the $CuIn_3Se_5$ phase has been considered as a Cu-deficient compound near surfaces and grain boundaries. However, despite intensive research,[23,24] a precise structural model for the $CuIn_3Se_5$ phase remains elusive, possibly due to inherent randomness[24] in the position of the Cu vacancies and In antisites (i.e., In on Cu sites). Consequently, modeling the electronic structure of the $CuIn_3Se_5$ phase is challenging. However, the stoichiometry of $CuIn_3Se_5$ is a weighted sum of the stoichiometry of $CuInSe_2$ and of $CuIn_5Se_8$; we will represent the density of states (DOS) of this phase accordingly. The simulated HAXPES spectra of the different compounds are obtained by summing up partial atom- and orbital-resolved densities of states (PDOSs) weighted by the corresponding theoretical free-atom photoionization cross sections.[25,26] Finally, we use linear combinations of these simulated spectra to fit the experimental spectra. On the basis of the fit results, we then attempt to identify the chemical origin of the main spectral valence band features and draw conclusions with respect to sample composition and how it changes upon KF-PDT.

2. METHODS

Our calculations were performed in the framework of DFT employing the HSE06[27,28] functional, as implemented in the FHI-aims code.[29] Electron wave functions were calculated by the full potential all-electron method. We employed primitive cells in all cases. The 8 × 8 × 8 *k*-point mesh was used for each structure.

The atomic orbital basis employed in FHI-aims provides a straightforward way to decompose the total density of states (DOS) into its atom- and orbital-projected contributions (PDOSs). To compare theoretical results with experimental HAXPES spectra, PDOSs were weighted with atom- and orbital-dependent photoionization cross sections (see Table S2). However, we modified the cross section of the In-d states within the valence band. In CIGSe, the atomic *In 4d* states form a narrow band at around 20 eV below VBM with well-localized wave functions and practically without hybridization with other atomic orbitals. However, in our calculations, the projection of valence band states onto the *In 4d* states is (although very small) nonzero, and thus using the very large *In 4d* photoionization cross section for these small projection components would cause remarkable artificial contributions close to VBM. The In-related states close to the Fermi level originate from hybridization of the atomic *In 5p* states, and therefore the expected small projection onto the *In 4d*states is combined with the projection on the *In 5p* states, i.e., we adopt the *In 5p* photoinization cross section value also for the *In 4d* states. Note that the findings on the valence band region presented below are rather independent of the projections onto the *In 4d* states (once their artificial photoionization cross section correction-induced significant overestimation is avoided) and thus their exact intensity correction for photoionization cross section effects is insignificant. After weighting by cross sections, PDOSs were convoluted with a Gaussian function of 0.3 eV in width to account for the thermal and instrumental broadening of the measurements. To get PDOSs per atom, all PDOSs were divided by the number of atoms in the unit cell. Then, the simulated HAXPES spectra were obtained by summing up all contributing weighted and convoluted PDOSs. By omitting the weighting, we obtained convoluted total DOSs, which we also show in the comparisons below.

3. RESULTS AND DISCUSSION

We first present the calculated valence band DOSs and the simulated HAXPES spectra for all potentially present phases and analyze the origin of the most prominent spectral features. This is followed by showing the fits to the experimental spectra and the discussion of the results.

DOI: 10.1021/acsami.8b18216
ACS Appl. Mater. Interfaces 2019, 11, 3024−3033

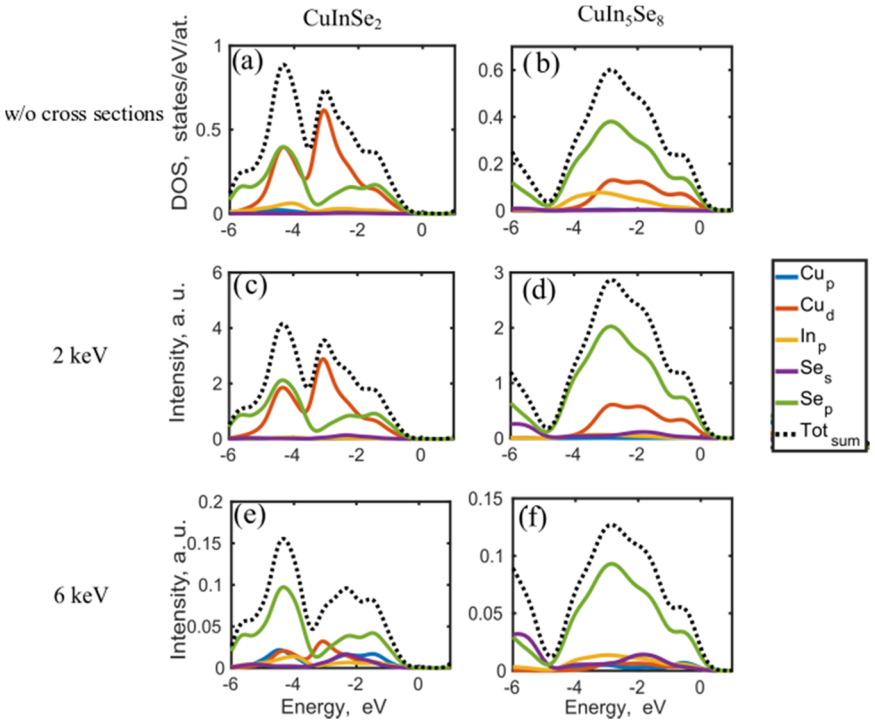

Figure 1. Total DOSs (dotted lines) and PDOSs (solid lines) for $CuInSe_2$ (a, c, e) and $CuIn_5Se_8$ (b, d, f), without photoionization cross section correction (a, b) and with correction for kinetic energies of 2 keV (c, d) and 6 keV (e, f), respectively. In all panels, the energy equal to zero coincides with the VBM position.

3.1. Densities of States of Relevant Cu Compounds. We start with the alkali-free CIGSe sample (i.e., no NaF/KF-PDT). The untreated absorber surface cannot be described as a stoichiometric $CuInSe_2$ but is found to have a significant Cu deficiency (indicating a surface stoichiometry between $CuIn_3Se_5$ and $CuIn_5Se_8$), confirming previous reports.[14,30−32] Such Cu-deficient CIGSe surfaces have been attributed to the formation of ordered defect/vacancy surface compounds (i.e., $CuIn_3Se_5$ and/or $CuIn_5Se_8$)[33,34] or surface reconstruction (i.e., a Cu-free In−Se-type surface termination) in the past.[35] One of the aims of this work is to contribute to this ongoing discussion. The more Cu-deficient $CuIn_5Se_8$ phase, first proposed by Zhang et al.[18] and afterward used, e.g., in the defect studies by Kiss et al.[36] and Ghorbani et al.,[37] has a stannite-type crystal structure with a periodic repetition of defect clusters of two Cu vacancies and an In-on-Cu antisite. As mentioned above, there exists no simple model for $CuIn_3Se_5$. However, we will represent the $CuIn_3Se_5$ DOS as a weighted sum of $CuInSe_2$ and $CuIn_5Se_8$ DOS for the comparison with HAXPES valence band spectra of the alkali-free CIGSe below.

The valence band DOSs for $CuInSe_2$ and $CuIn_5Se_8$ are shown in Figure 1a,b, respectively. It can be seen that they are dominated by *Cu d* and *Se p* states, which are distributed quite differently in the two materials. For $CuInSe_2$, the two main peaks in DOS arise from bonding and antibonding states between *Cu d* and *Se p*. In the ordered defect compound $CuIn_5Se_8$, the deficiency of Cu obviously leads to the deficiency of Cu−Se bonds. As a result, the region of hybridized *Cu d* and *Se p* states narrows so that the two prominent peaks in the total DOS merge and the total bandwidth decreases, in agreement with ref 18. Figure 1c,e shows the $CuInSe_2$ PDOSs multiplied by the photoionization cross sections for electrons having a kinetic energy of 2 and 6 keV, respectively, thus approximating the corresponding HAXPES spectra. The total relative intensities of the two main peaks are equal for the spectra without photoionization cross section weighting and with 2 keV cross section correction (Figure 1a,c). In Figure 1c, the shoulder near the VBM comprises nearly equal *Se p* and *Cu d* contributions and the peak between −2.5 and −1.5 eV is prominently formed by *Cu d* orbitals. For the 6 keV cross section-weighted DOS (Figure 1e), the contribution of the *Cu d* orbital is significantly reduced and the *p*- and *s*-derived contributions increase in intensity. As a result, the *Cu p*- and *Se p*-derived low-energy DOS becomes relatively more intense. For $CuIn_5Se_8$ (see Figure 1b,d,f), the uncorrected total DOS and the 2 keV cross section-weighted DOS are very similar, as in the case of the $CuInSe_2$. For the 6 keV cross section correction, the *Cu d* contribution again is reduced and the *p*- and *s*-derived orbitals increase in intensity.

3.2. Densities of States of Relevant (K−)In−Se Compounds. The microscopic character of the surface modification of the CIGSe absorber material after the KF-PDT has been discussed extensively during recent years.[3,4,12,17] Possible reasons for the surface modifications could be the formation of K−In−Se[8,13,15−17,20,38] and/or In−Se-type layers.[16,17,38] In this work, we consider $KInSe_2$ in two different lattice structures (monoclinic and chalcopyrite-type) as well as In_2Se_3 and InSe as being the phases that most likely form at the absorber surface.

Our previous calculations[23] suggested that K can fill up pre-existing Cu vacancies during KF-PDT, but on the basis of formation enthalpies, the resulting alloy would undergo phase separation to $CuInSe_2$ and $KInSe_2$ phases if the process is kinetically feasible. Reordering of the Cu and K would then naturally lead to the formation of chalcopyrite $KInSe_2$. Experimentally, the stable $KInSe_2$ phase is monoclinic, with a layered atomic structure.[23] As the calculated formation

DOI: 10.1021/acsami.8b18216
ACS Appl. Mater. Interfaces 2019, 11, 3024−3033

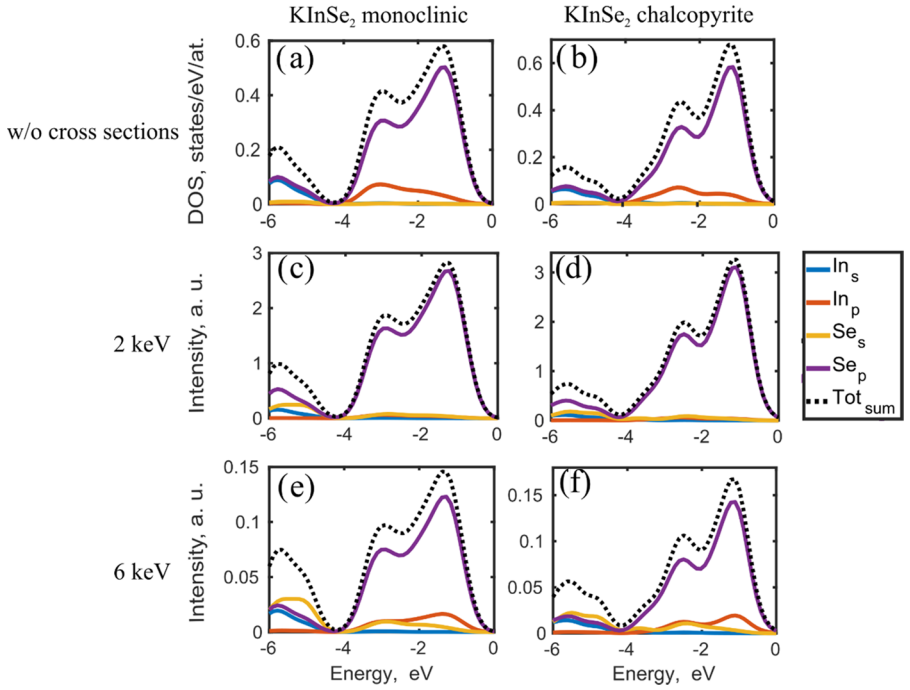

Figure 2. Total DOSs (dotted lines) and PDOSs (solid lines) for monoclinic (a, c, e) and chalcopyrite-type $KInSe_2$ (b, d, f), without photoionization cross section correction (a, b) and with correction for kinetic energies of 2 keV (c, d) and 6 keV (e, f), respectively. In all panels, the energy equal to zero coincides with the VBM position. Note that the K contributions are vanishingly small within the energy region shown and thus are not included.

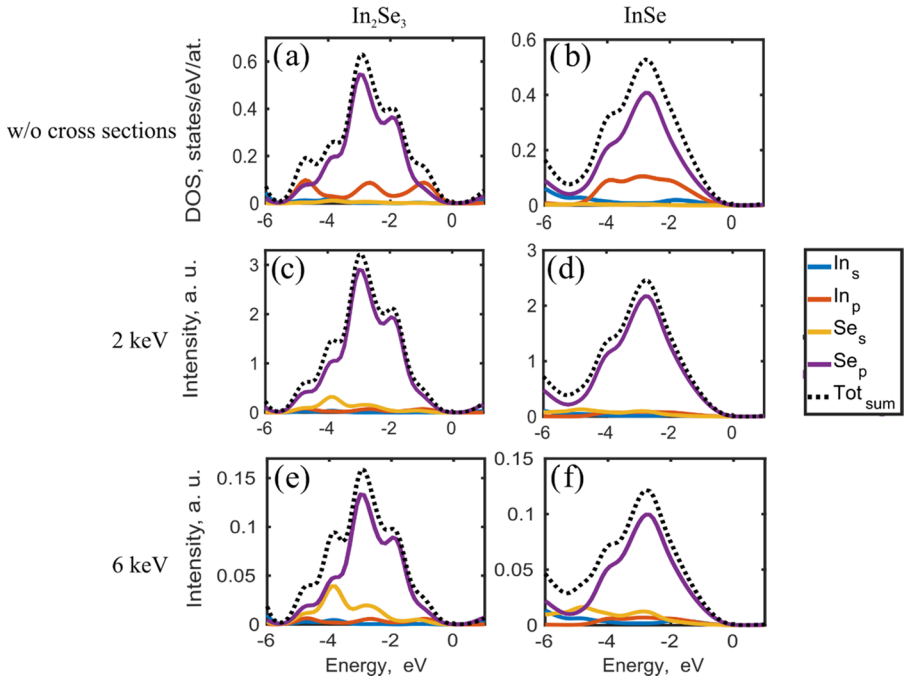

Figure 3. Total DOSs (dotted lines) and PDOSs (solid lines) for In_2Se_3 (a, c, e) and InSe (b, d, f), without photoionization cross section correction (a, b) and with correction for kinetic energies of 2 keV (c, d) and 6 keV (e, f), respectively. In all panels, the energy equal to zero coincides with the VBM position.

enthalpies for the two phases are similar, differing only by 0.13 eV, both phases are considered in the following discussion.

The valence band DOSs for both $KInSe_2$ polymorphs are shown in Figure 2a,b. They are dominated mainly by the *Se p* features, with a minor *In p* contribution seen between 0 and −4 eV. There is no significant contribution from K-derived orbitals to the valence band DOSs, reflecting the ionic character of K in the compound. The photoionization cross section-weighted DOSs for 2 keV and both types of $KInSe_2$ are (almost) exclusively due to the *Se p* orbital; see Figure 2c,d. For the 6 keV correction shown in Figure 2e,f *In p* and *In s/Se s* contributions become more pronounced. However, since the two $KInSe_2$ structures contain similar InSe skeletons with ionized K atoms only providing extra electrons, the (weighted)

DOI: 10.1021/acsami.8b18216
ACS Appl. Mater. Interfaces 2019, 11, 3024−3033

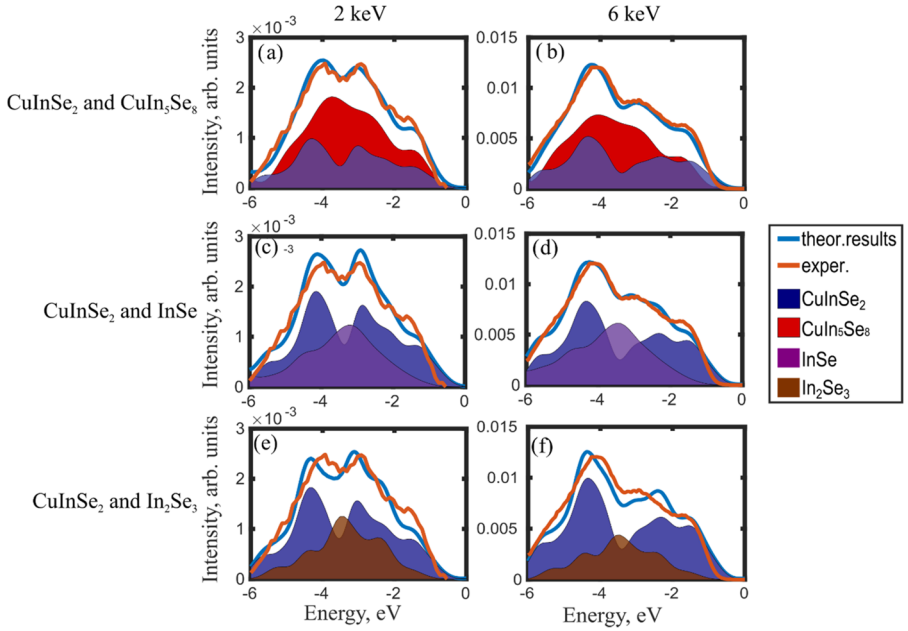

Figure 4. Photoionization cross section-corrected DOSs and experimental HAXPES spectra for the alkali-free CIGSe sample measured with excitation energies of 2 (a, c, e) and 6 keV (b, d, f). The components used for the fit are given on the left. The fraction of the calculated, corrected DOS components to give the best fit (for the respective compound combination) are displayed as filled areas under the curves. The respective goodness of the fit together with other fit parameters are stated in Table 1.

DOSs for the two polymorphs are very similar, making it difficult to differentiate between them in the HAXPES spectra. This also means that it is possible to use either one when fitting the experimental spectra below. Since the formation of monoclinic, layered $KInSe_2$ is energetically more favorable (see Section 3), this phase was used in the considerations below.

We consider in this work the α-phase of In_2Se_3 and the γ-phase of InSe. According to our calculations, they have lower formation enthalpies than other In−Se phases and similarly to the case of $KInSe_2$ polymorphs, we do not expect significant differences between phases of the same stoichiometry. In_2Se_3 DOSs (without and with photoionization cross section correction) are shown in Figure 3a,c,e, and those for InSe, in Figure 3b,d,f. They are dominated by pronounced peaks between −4.5 and −1.5 eV, which are due to the *Se p* orbital similar to the potassium indium selenides considered above. Within the energy range from −6 to 0 eV, the main contributions in the DOS are due to the *Se p* and *In p* orbitals. The hybridization of the orbitals (bond formation) is, however, not strong as can be inferred from the very different intensities of the two contributions. The hybridization results in shoulders on both sides of the DOS main peak in the case of In_2Se_3, whereas only one shoulder at the higher binding energy side appears in the case of InSe. In the 2 keV photoionization cross section-weighted DOS, the *Se p* feature dominates without any significant contributions from other orbitals. The 6 keV corrected DOSs look mainly the same, with a small increase of the *In p* and Se_s contributions.

3.3. Comparison of Computed DOSs with HAXPES Spectra. Even without fitting one can immediately recognize obvious resemblances between the computed and photoionization cross section-weighted DOSs of $CuInSe_2$ or $CuIn_5Se_8$ and the experimental HAXPES spectra of the alkali-free CIGSe sample shown in Figure S1. Similarly, the experimental spectra of the K-rich samples show strong similarities with the computed and weighted $KInSe_2$ as well as InSe DOSs. These observations form the "basis set" for the materials used in the fitting procedure, aiming at representing the experimental HAXPES spectra by a combination of calculated, photoionization cross section-corrected DOSs.

The total corrected DOSs are modeled as linear combinations of the respective DOSs for all contributing phases. i.e.

$$g_{tot}(E) = \sum_i a_i g_i(E - b_i) \quad (1)$$

where g_i is the cross section-corrected DOS for sample component i and a_i is its concentration. The shifts b_i along the energy axis E account for the expected different energy level positions with respect to the experimental spectrum. The coefficients a_i and b_i were determined by minimizing the mean square error between experimental and simulated intensities. The goodness of the fitting was obtained relative to the normalized mean square error of the fit as

$$G = 1 - \frac{\| g_{ref}(E) - g_{tot}(E) \|}{\| g_{ref}(E) - \langle g_{ref}(E) \rangle_E \|} \quad (2)$$

where g_{ref} is a HAXPES data vector, $\langle \rangle_E$ gives the mean value of the data, and ||...|| indicates the 2-norm of a vector. Thus, the closer G is to unity, the better is the fit. To obtain as meaningful fits as possible, we kept the fitting parameters to a minimum and assumed that each experimental spectra is constituted of a maximum of two phases, leading to four fitting parameters for each fit.

3.3.1. Alkali-Free CIGSe Absorber. We assume that the alkali-free CIGSe absorber (surface) is composed of $CuInSe_2$, $CuIn_5Se_8$, InSe, and/or In_2Se_3 phases and the respective HAXPES spectra can be represented as a linear combination of these components. Results of the fits of the experimental spectrum corresponding to the 2 keV excitation energy using the photoionization cross section-corrected DOSs for different components are shown in the left hand side column of Figure

DOI: 10.1021/acsami.8b18216
ACS Appl. Mater. Interfaces 2019, 11, 3024−3033

Table 1. Fitting Results for the Alkali-Free CIGSe Sample Measured with Excitation Energies of 2 and 6 keV[a]

phases in fit		2 keV data			6 keV data		
A	B	intensity ratio	band offset (eV)	G	intensity ratio	band offset (eV)	G
$CuInSe_2$	$CuIn_5Se_8$	27:73	−0.3	0.86	37:63	−0.5	0.86
$CuInSe_2$	InSe	47:53	−0.5	0.78	52:47	−0.7	0.77
$CuInSe_2$	In_2Se_3	53:47	−0.7	0.77	70:30	−0.4	0.75

[a]The components (A, B) used in the fit are given in the first column. The ratios of the resulting component intensities (I(A)/I(B)) and the band offsets, i.e., the VBM difference (VBM(B) − VBM(A)) are given next. G, the goodness of the fit (as defined in eq 2) is also stated.

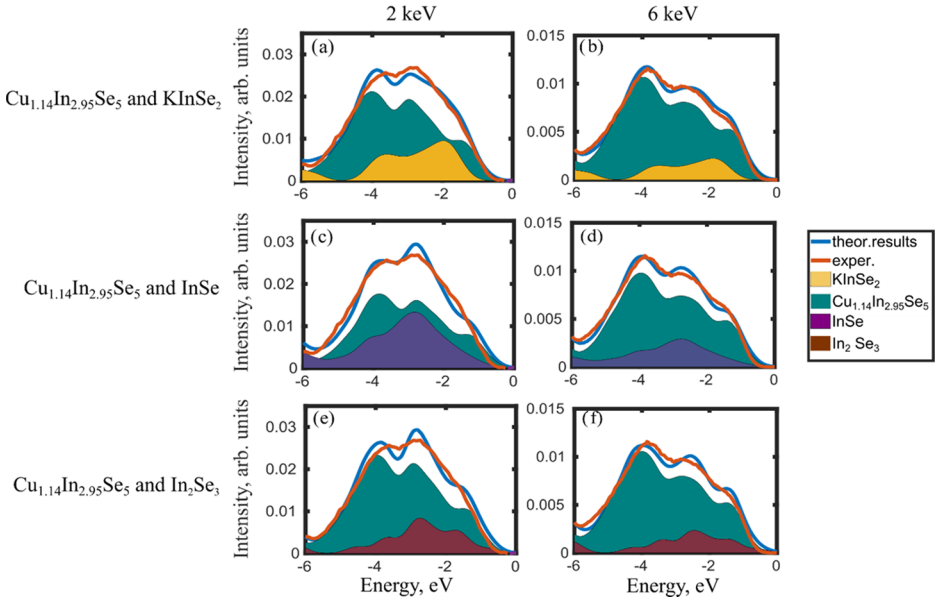

Figure 5. Photoionization cross section-corrected DOSs and experimental HAXPES spectra for K-poor CIGSe samples measured with excitation energies of 2 (a, c, e) and 6 keV (b, d, f). The components used for the fit are given on the left of the column. The fraction of the calculated, corrected DOS components to give the best fit (for the respective compound combination) are displayed as filled areas under the curves. The respective goodness of the fit together with other fit parameters is stated in Table 2.

4. Numerical data of the fits are given in Table 1. The experimental spectra shown in Figure 4a,b are best fit when a valence band offset of −0.3 and −0.5 eV is used between $CuInSe_2$ and $CuIn_5Se_8$, i.e., the VBM of $CuIn_5Se_8$ is at lower energy. The band offset is similar to a suggested value of −0.55 eV for the interface between $CuInSe_2$ and the ordered vacancy compound (ref 33). The uncertainties related to DOS calculations and DFT energy level structures, as well as to the experimental resolution limit the accuracy of our band offset determination and we give them using only one digit. However, the qualitative consistency of the band offsets and the overall good agreement to experiments, including the shapes and the widths of the valence band spectra, give confidence to our modeling approach, both with respect to the selected phases (and their atomic structures) and the HAXPES simulation approach.

The quality of the respective fits of the 2 and 6 keV HAXPES data (Figure 4a,b) is best for the $CuInSe_2$−$CuIn_5Se_8$ combination. According to Table 1, the $CuInSe_2$/$CuIn_5Se_8$ composition ratio for the 2 keV excitation is 27:73 and for the 6 keV excitation 37:63. Thus, the Cu-deficient phase has a larger relative contribution for the more surface sensitive HAXPES data, in agreement with previous findings.[13] The fit component ratios can be used to calculate chemical formulae as follows: The different atomic percentages in the $CuInSe_2$ and $CuIn_5Se_8$ phases are weighted by the derived component ratios and normalized to five Se atoms. The 2 and 6 keV composition ratios then result in $Cu_{1.08}In_{2.97}Se_5$ and $Cu_{1.26}In_{2.91}Se_5$ stoichiometries, respectively. Thus, closest to the surface, the stoichiometry is very close to that of $CuIn_3Se_5$ and deeper into the material, the Cu content increases (valence electron IMFPs for 2 and 6 keV excitations are 4 and 10 nm, respectively). For the $CuInSe_2$−InSe (Figure 4c,d) and $CuInSe_2$−In_2Se_3 (Figure 4e,f) combinations, the quality of the fits is lower, especially around the intensity maxima and close to VBM. Note that the linear combination of In_2Se_3 and $CuInSe_2$ can also produce the stoichiometry of a Cu-deficient phase such as $CuIn_3Se_5$; however, our fitting results favor a $CuInSe_2$−$CuIn_5Se_8$ composition at the surface. However, the relatively large IMFP of even the 2 keV excited measurements means that a Cu-free surface reconstruction[35] of a few angstroms at the CIGSe surface would be effectively invisible within the signal-to-noise ratio of the measurements and the uncertainty in the analysis approach.

3.3.2. K-Poor CIGSe Absorber. HAXPES spectrum fits of the K-poor sample measured with the 2 and 6 keV excitation energies are presented in Figure 5. To represent the measured data, on the basis of our findings for the alkali-free sample discussed above, we use for the substrate an average $CuInSe_2$/$CuIn_5Se_8$ composition ratio of 30:70, resulting in the formula $Cu_{1.14}In_{2.95}Se_5$ and the mean band offset of −0.4 eV. However, note that the results for KF-PDT-treated samples are not very sensitive to the substrate stoichiometry. Then, the photoionization cross section-corrected DOSs of this substrate are

DOI: 10.1021/acsami.8b18216
ACS Appl. Mater. Interfaces 2019, 11, 3024−3033

Table 2. Fitting Results for the K-Poor CIGSe Sample Measured with Excitation Energies of 2 and 6 keV[a]

phases in fit		2 keV data			6 keV data		
A	B	intensity ratio	band offset (eV)	G	intensity ratio	band offset (eV)	G
$Cu_{1.14}In_{2.95}Se_5$	$KInSe_2$	67:33	−0.5	0.87	84:16	−0.6	0.89
$Cu_{1.14}In_{2.95}Se_5$	InSe	52:48	−0.1	0.83	77:23	−0.3	0.88
$Cu_{1.14}In_{2.95}Se_5$	In_2Se_3	75:25	−0.1	0.83	85:15	−0.2	0.85

[a]The components (A, B) used in the fit are given in the first column. The ratios of the resulting component intensities (I(A)/I(B)) and the band offsets, i.e., the VBM difference (VBM(B) − VBM(A)) are given next. G the goodness of the fit (as defined in eq 2) is also stated.

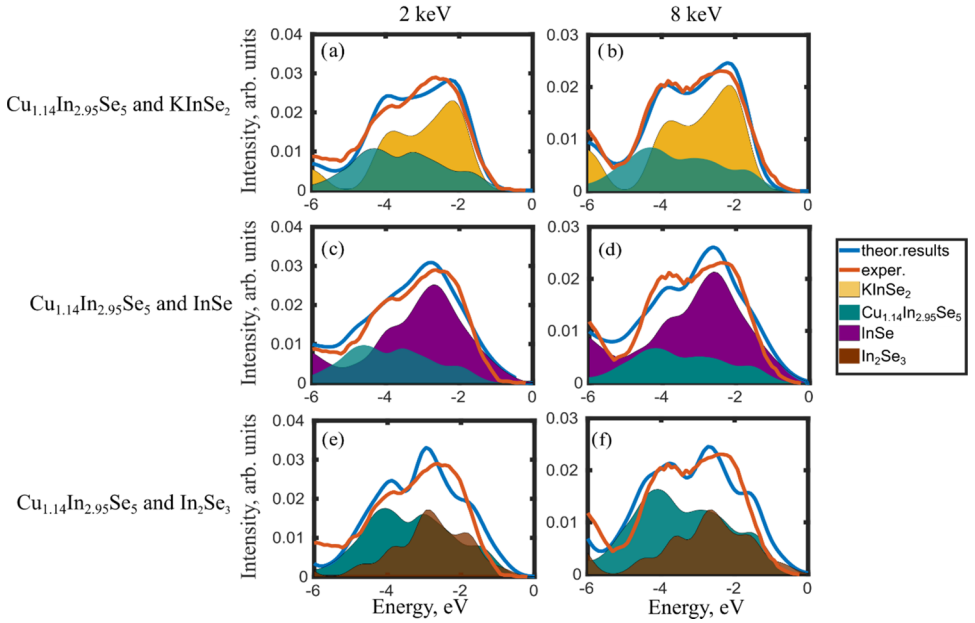

Figure 6. Photoionization cross section-corrected DOSs and experimental HAXPES spectra for K-rich CIGSe samples measured with excitation energies of 2 (a, c, e) and 8 keV (b, d, f). The components used for the fit are given on the left of the column. The fraction of the calculated, corrected DOS components to give the best fit (for the respective compound combination) are displayed as filled areas under the curves. The respective goodness of the fit together with other fit parameters are stated in Table 3.

Table 3. Fitting Results for the K-Rich CIGSe Sample Measured with Excitation Energies of 2 and 8 keV[a]

phases in fit		2 keV data			6 keV data		
A	B	intensity ratio	band offset (eV)	G	intensity ratio	band offset (eV)	G
$Cu_{1.14}In_{2.95}Se_5$	$KInSe_2$	70:30	−0.5	0.81	68:32	−0.5	0.86
$Cu_{1.14}In_{2.95}Se_5$	InSe	76:24	0.5	0.78	76:24	0.6	0.72
$Cu_{1.14}In_{2.95}Se_5$	In_2Se_3	48:52	0.1	0.64	38:62	0.4	0.64

[a]The components (A, B) used in the fit are given in the first column. The ratios of the resulting component intensities (I(A)/I(B)) and the band offsets, i.e., the VBM difference (VBM(B) − VBM(A)), are given next. G the goodness of the fit (as defined in eq 2) is also stated.

combined with those of the $KInSe_2$, InSe, or In_2Se_3 secondary phase components (cf. the first, second, and third row in Figure 5).

All simulated spectra have similar appearances due to the major $Cu_{1.14}In_{2.95}Se_5$ contribution describing well the main features. As given in Table 2, all material combinations show rather similar fit qualities although the fits using the $KInSe_2$ phase are the best. The mutual band offsets given indicate that VBMs of the secondary phases are below the VBM of the substrate, reflecting the effect of Cu 3*d* levels pushing the VBM upward in the substrate. The substrate contributions dominate in the fits, and they increase clearly from 2 to 6 keV excitation, i.e., on enhancing the information depth. Overall, the fitting confirms the surface modification and likely formation of a secondary phase with a pronounced (K−)In−Se bond contribution, but its contribution in the spectra is too small to reliably determine its composition.

3.3.3. K-Rich CIGSe Absorber. The HAXPES spectra and their fits for the K-rich CIGSe absorber are shown in Figure 6. Note that excitation energies of 2 and 8 keV were used for these samples instead of the 2 and 6 keV used for the alkali-free and K-poor CIGSe sample discussed above. The shapes of the 6 and 8 keV photoionization cross section-corrected DOSs for the different phases we consider are very similar, but the DOSs corrected for the 8 keV photoionization cross sections have only about 50% of the 6 keV intensity (see Table S2). The substrate is again $Cu_{1.14}In_{2.95}Se_5$. Compared to the K-poor results, the intensities of the spectra below VBM have considerably increased but appear to retain an otherwise similar shape. A linear combination of the photoionization cross section-corrected DOSs of $Cu_{1.14}In_{2.95}Se_5$ and $KInSe_2$

DOI: 10.1021/acsami.8b18216
ACS Appl. Mater. Interfaces 2019, 11, 3024−3033

yields clearly the best match with the 2 keV as well as the 8 keV experimental spectra of the K-rich CIGSe absorber. Moreover, the derived band offsets between these two phases are consistent in all cases, as shown in Tables 2 and 3, further supporting the reliability of our fitting procedure. By comparison, the fits with InSe and In_2Se_3 cannot reproduce the shapes of the measured spectra. Most striking is, however, the inconsistency of the derived band offsets switching from being negative for the alkali-poor to positive for the alkali-rich sample set. Considering that both phases are supposed to have a larger band gap energy than that of (even Cu-deficient) CIGSe material (i.e., $Cu_{1.14}In_{2.95}Se_5$) and that In−Se variants are generally n-type (at least compared to CIGSe or $Cu_{1.14}In_{2.95}Se_5$), a positive band offset is not reasonable and thus a clear indication for the KF-PDT-induced formation of a K−In−Se instead of InSe and In_2Se_3-type species.

By comparing the $KInSe_2$ fits for the absorbers of different KF-PDT rates in Figures 5 and 6 and Tables 2 and 3, it can be concluded that with the increasing KF exposure, the volume of the secondary phase increases whereas that of the substrate compound diminishes. Moreover, for the K-poor sample, the increase of the excitation energy increases remarkably the secondary phase contribution, whereas for the K-rich sample, the increase is modest, at most. The $KInSe_2$ volume share would, due to its open layered structure and lower atomic density, be larger than its atomic contribution, e.g., for the K-rich sample, more than about 70%. Although the above two very clear trends are obvious and thereby confirm the robustness of our comparison as an analyzing scheme, we do not want to make quantitative estimates about the relative abundances because of the related uncertainties, such as the well-known limitations of DFT to describe the electron energy level structures and also more practical issues such as the use of free-atom cross sections and projection method of our theoretical construction. Regarding the identity of the secondary phase, the use of the $KInSe_2$ phase results consistently in the best fits throughout our sample series. However, it should also be considered that the formation of a pronounced K−In−Se type surface species on KF-PDT CIGSe absorbers might very well crucially depend on the K amount used in the PDT.

The formation of a K−In−Se-type secondary phase at the surface of CIGSe thin-film solar cell absorbers has certainly consequences for the electronic interface structure to the emitter of the solar cell device. The optoelectronic properties of this phase significantly differ from those of CIGSe. Most prominently, the band gap energy is supposedly larger than that of (even Cu-deficient) CIGSe material,[17] and interestingly is in the range of that reported for CdS. Because KF-PDT allows for the deposition of thinner CdS buffer layers, optical losses are reduced and higher short circuit currents of respective solar cell devices are achieved.[4] The presence of K−In−Se type surface species on KF-PDT CIGSe absorbers may also affect (and thus opens a route to deliberately tune) the energy level alignment at the buffer/absorber heterointerface. The observed lowering of the VBM (i.e., away from E_F) even compared to that of Cu-deficient CIGSe might increase the charge selectivity of the CdS/CIGSe contact (repelling holes from the heterointerface), thus reducing high-rate charge carrier interface recombination.

4. CONCLUSIONS

We have analyzed HAXPES spectra of CIGSe solar cell absorbers exposed to NaF/KF-PDT using linear combinations of simulated spectra for Cu-deficient CIGSe phases of different stoichiometries and of potentially formed secondary phases, such as $KInSe_2$, InSe, and In_2Se_3. HAXPES data of K-poor and K-rich samples measured with X-ray excitation energies of 2, 6, and 8 keV were used for comparison. Samples without PDT were used as alkali-free CIGSe references. Although the crystalline structure of the surfaces of the samples is not known, our method allows us to derive a first-principles description of the electronic structure of their valence bands. Our analyses give robust trends and enable us to draw conclusions for the different samples and for the 2 and 6 (8) keV HAXPES data having different probing depths. The most important findings are: (i) The surface of alkali-free CIGSe is Cu depleted. The HAXPES valence band spectra are best described by a mixture of the (photoionization cross section) corrected DOS of stoichiometric $CuInSe_2$ and Cu-deficient $CuIn_5Se_8$ with the resulting stoichiometry at the surface corresponding roughly to $CuIn_3Se_5$, being less Cu-deficient further away from the surface. The combinations involving Cu-free In−Se compounds did not result in reasonable fits of the measured valence band spectra (without additional Cu-containing phases). This could indicate the presence of an ordered defect/vacancy surface compound.[32,33] (ii) The valence band structure of K-rich samples agrees well with a superposition of corrected $KInSe_2$ and Cu-deficient phase DOSs. (iii) The valence band of K-poor samples can also be explained by a combination of $KInSe_2$ and the Cu-deficient phase. However, explaining the valence band structure by a corrected DOS combination of In−Se-type species (and here, in particular, In_2Se_3) and a Cu-deficient phase such as $CuIn_3Se_5$ results in a similar fit quality, indicating that the formation of a pronounced K−In−Se-type species might depend on the K amount available during PDT. In any case, (K)In−Se-type surface phases have different optoelectronic properties than those of (Cu-deficient) CIGSe. To what extent this will affect the electronic structure at the emitter/absorber heterointerface in the thin-film device layer stack is a subject of ongoing studies and discussions.

■ ASSOCIATED CONTENT

Supporting Information

The Supporting Information is available free of charge on the ACS Publications website at DOI: 10.1021/acsami.8b18216.

HAXPES spectra for K-free, K-poor, and K-rich samples; photoionization cross sections for Cu-, In-, Se-, and K-derived valence orbitals; crystal structures of the calculated phases (PDF)

■ AUTHOR INFORMATION

Corresponding Author

*E-mail: martti.puska@aalto.fi.

ORCID

Hannu-Pekka Komsa: 0000-0002-0970-0957
Evelyn Handick: 0000-0002-9773-9981
Marcus Bär: 0000-0001-8581-0691
Martti J. Puska: 0000-0002-8419-3289

Notes

The authors declare no competing financial interest.

DOI: 10.1021/acsami.8b18216
ACS Appl. Mater. Interfaces 2019, 11, 3024−3033

■ ACKNOWLEDGMENTS

The project has received funding from the European Union's Horizon 2020 research and innovation program under the grant agreement No. 641004 (Sharc25). We acknowledge the generous computational resources provided by the CSC supercomputer center of Finland and also by the Aalto Science-IT project. The authors would also like to thank our partners from the Laboratory of Thin Films and Photovoltaics at EMPA (Swiss Federal Laboratories for Materials Science and Technology), the Institut für Physik and IRIS Adlershof at Humboldt-Universität zu Berlin, the SPring-8/JASRI, and BESSY II/HZB for their contributions to the article "Potassium Postdeposition Treatment-Induced Band Gap Widening at Cu(In,Ga)Se_2 Surfaces—Reason for Performance Leap?" in "ACS Applied Materials & Interfaces",[17] which initiated this work.

■ REFERENCES

(1) Stanbery, B. J. Copper Indium Selenides and Related Materials for Photovoltaic Devices. *Crit. Rev. Solid State Mater. Sci.* **2002**, *27*, 73−117.

(2) Repins, I.; Contreras, M. A.; Egaas, B.; DeHart, C.; Scharf, J.; Perkins, C. L.; To, B.; Noufi, R. 19.9%-efficient ZnO/CdS/$CuInGaSe_2$ Solar Cell with 81.2% Fill Factor. *Prog. Photovoltaics* **2008**, *16*, 235−239.

(3) Chirilă, A.; Reinhard, P.; Pianezzi, F.; Blösch, P.; Uhl, A. R.; Sutter-Fella, C.; Kranz, L.; Keller, D.; Gretener, C.; Hagendorfer, H.; Jaeger, D.; Erni, R.; Nishiwaki, S.; Buecheler, S.; Tiwari, A. N. Potassium-Induced Surface Modification of Cu(In,Ga)Se_2 Thin Films for High-Efficiency Solar Cells. *Nat. Mater.* **2013**, *12*, 1107−1111.

(4) Reinhard, P.; Bissig, B.; Pianezzi, F.; Hagendorfer, H.; Sozzi, G.; Menozzi, R.; Gretener, C.; Nishiwaki, S.; Buecheler, S.; Tiwari, A. N. Alkali-Templated Surface Nanopatterning of Chalcogenide Thin Films: A Novel Approach Toward Solar Cells with Enhanced Efficiency. *Nano Lett.* **2015**, *15*, 3334−3340.

(5) Reinhard, P.; Bissig, B.; Pianezzi, F.; Avancini, E.; Hagendorfer, H.; Keller, D.; Fuchs, P.; Döbeli, M.; Vigo, C.; Crivelli, P.; Nishiwaki, S.; Buecheler, S.; Tiwari, A. N. Features of KF and NaF Postdeposition Treatments of Cu(In,Ga)Se_2 Absorbers for High Efficiency *Thin Film Solar Cells. Chem. Mater.* **2015**, *27*, 5755−5764.

(6) Jackson, P.; Hariskos, D.; Lotter, E.; Paetel, S.; Wuerz, R.; Menner, R.; Wischmann, W.; Powalla, M. New World Record Efficiency for Cu(In,Ga)Se_2 Thin-Film Solar Cells Beyond 20%. *Prog. Photovoltaics* **2011**, *19*, 894−897.

(7) Jackson, P.; Hariskos, D.; Wuerz, R.; Wischmann, W.; Powalla, M. Compositional Investigation of Potassium Doped Cu(In,Ga)Se_2 Solar Cells with Efficiencies up to 20.8%. *Phys. Status Solidi RRL* **2014**, *8*, 219−222.

(8) Kato, T. Cu(In,Ga)$(Se,S)_2$ Solar Cell Research in Solar Frontier: Progress and current status. *Jpn. J. Appl. Phys.* **2017**, *56*, No. 04CA02.

(9) Jackson, P.; Wuerz, R.; Hariskos, D.; Lotter, E.; Witte, W.; Powalla, M. Effects of Heavy Alkali Elements in Cu(In,Ga)Se_2 Solar Cells with Efficiencies up to 22.6%. *Phys. Status Solidi RRL* **2016**, *10*, 583−586.

(10) Jyh-Lih, W.; Yoshiaki, H.; Takuya, K.; Hiroki, S.; Veronica, B. In *New World Record Efficiency up to 22.9% for Cu(In,Ga)$(Se,S)_2$ Thin-Film Solar Cells*, Presented at 7th World Conference on Photovoltaic Energy Conversion, Waikoloa, Hawaii, 2018.

(11) Laemmle, A.; Wuerz, R.; Powalla, M. Efficiency Enhancement of Cu(In,Ga)Se_2 Thin-Film Solar Cells by a Post-Deposition Treatment with Potassium Fluoride. *Phys. Status Solidi RRL* **2013**, *7*, 631−634.

(12) Muzzillo, C. P. Review of Grain Interior, Grain Boundary, and Interface Effects of K in CIGS Solar Cells: Mechanisms for Performance Enhancement. *Sol. Energy Mater. Sol. Cells* **2017**, *172*, 18−24.

(13) Handick, E.; Reinhard, P.; Wilks, R. G.; Pianezzi, F.; Kunze, T.; Kreikemeyer-Lorenzo, D.; Weinhardt, L.; Blum, M.; Yang, W.; Gorgoi, M.; Ikenaga, E.; Gerlach, D.; Ueda, S.; Yamashita, Y.; Chikyow, T.; Heske, C.; Buecheler, S.; Tiwari, A. N.; Bär, M. Formation of a K-In-Se Surface Species by NaF/KF Postdeposition Treatment of Cu(In,Ga)Se_2 Thin-Film Solar Cell Absorbers. *ACS Appl. Mater. Interfaces* **2017**, *9*, 3581−3589.

(14) Mezher, M.; Mansfield, L. M.; Horsley, K.; Blum, M.; Wieting, R.; Weinhardt, L.; Ramanathan, K.; Heske, C. KF Post-Deposition Treatment of Industrial Cu(In, Ga)$(S, Se)_2$ Thin-Film Surfaces: Modifying the Chemical and Electronic Structure. *Appl. Phys. Lett.* **2017**, *111*, No. 071601.

(15) Handick, E.; Reinhard, P.; Wilks, R. G.; Pianezzi, F.; Félix, R.; Gorgoi, M.; Kunze, T.; Buecheler, S.; Tiwari, A. N.; Bär, M. In *NaF/KF Post-Deposition Treatment and Their Influence on the Structure of Cu(In,Ga)Se_2 Absorber Surfaces*, 2016 IEEE 43rd Photovoltaic Specialists Conference (PVSC), Portland, OR, 0017-0021, 2016.

(16) Lepetit, T.; Harel, S.; Arzel, L.; Ouvrard, G.; Barreau, N. Coevaporated $KInSe_2$: A Fast Alternative to KF Postdeposition Treatment in High-Efficiency Cu(In,Ga)Se_2 Thin Film Solar Cells. *IEEE J. Photovoltaics* **2016**, *6*, 1316−1320.

(17) Handick, E.; Reinhard, P.; Alsmeier, J.-H.; Köhler, L.; Pianezzi, F.; Krause, S.; Gorgoi, M.; Ikenaga, E.; Koch, N.; Wilks, R. G.; Buecheler, S.; Tiwari, A. N.; Bär, M. Potassium Postdeposition Treatment-Induced Band Gap Widening at Cu(In,Ga)Se_2 Surfaces - Reason for Performance Leap? *ACS Appl. Mater. Interfaces* **2015**, *7*, 27414−27420.

(18) Zhang, S. B.; Wei, S.-H.; Zunger, A.; Katayama-Yoshida, H. Defect Physics of the $CuInSe_2$ Chalcopyrite Semiconductor. *Phys. Rev. B: Condens. Matter Mater. Phys.* **1998**, *57*, 9642−9656.

(19) Kish, Z. Z.; Peresh, E. Y.; Lazarev, V. B.; Semrad, E. E. Systematics and the Rules of Variations in the Properties of the $A^{I}B^{III}C_2^{VI}$-Type Compounds. *Izv. Akad. Nauk SSSR, Neorg. Mater.* **1987**, *23*, 777.

(20) Lazarev, V. B; Kish, Z. Z.; Peresh, E. Y.; Semrad, E. E. *Complex Chalcogenides in the A^{I}−B^{III}−C^{VI} Systems*; Metallurgiya: Moscow, 1993.

(21) Handick, E. Surface and Interface Characterization by X-ray and Electron Spectroscopies − Revealing the Peculiarities of Cu(In,Ga)Se_2 Chalcopyrite and $CH_3NH_3PbI_{(3\,x)}Cl_x$ Perovskite-Based Thin Film Solar Cell Structures. Doctoral thesis, BTU Cottbus: Senftenberg, 2017.

(22) Tanuma, S.; Powell, C. J.; Penn, D. R. Calculations of Electron Inelastic Mean Free Paths. V. Data for 14 Organic Compounds over the 50−2000 eV *Range. Surf. Interface Anal.* **1994**, *21*, 165−176.

(23) Malitckaya, M.; Komsa, H.-P.; Havu, V.; Puska, M. J. Effect of Alkali Metal Atom Doping on the $CuInSe_2$-Based Solar Cell Absorber. *J. Phys. Chem. C* **2017**, *121*, 15516−15528.

(24) Chang, C.-H.; Wei, S.-H.; Johnson, J. W.; Zhang, S. B.; Leyarovska, N.; Bunker, G.; Anderson, T. J. Local structure of $CuIn_3Se_5$: X-ray Absorption Fine Structure Study and First-Principles Calculations. *Phys. Rev. B* **2003**, *68*, No. 054108.

(25) Trzhaskovskaya, M.; Nefedov, V.; Yarzhemsky, V. Photoelectron Angular Distribution Parameters for Elements z = 1 to z = 54 in the Photoelectron Energy Range 100−5000 eV. *At. Data Nucl. Data Tables* **2001**, *77*, 97−159.

(26) Trzhaskovskaya, M.; Nikulin, V.; Nefedov, V.; Yarzhemsky, V. Non-Dipole Second Order Parameters of the Photoelectron Angular Distribution for Elements Z = 1−100 in the Photoelectron Energy Range 1−10 keV. *At. Data Nucl. Data Tables* **2006**, *92*, 245−304.

(27) Heyd, J.; Scuseria, G. E.; Ernzerhof, M. Hybrid Functionals Based on a Screened Coulomb Potential. *J. Chem. Phys.* **2003**, *118*, 8207−8215.

(28) Ren, X.; Rinke, P.; Blum, V.; Wieferink, J.; Tkatchenko, A.; Sanfilippo, A.; Reuter, K.; Scheffler, M. Resolution-Of-Identity Approach to Hartree - Fock, Hybrid Density Functionals, RPA, MP2 and GW with Numeric Atom - Centered Orbital Basis Functions. *New J. Phys.* **2012**, *14*, No. 053020.

DOI: 10.1021/acsami.8b18216
ACS Appl. Mater. Interfaces 2019, 11, 3024−3033

(29) Blum, V.; Gehrke, R.; Hanke, F.; Havu, P.; Havu, V.; Ren, X.; Reuter, K.; Schffler, M. Ab Initio Molecular Simulations with Numeric Atom-Centered Orbitals. *Comput. Phys. Commun.* **2009**, *180*, 2175−2196.
(30) Morkel, M.; Weinhardt, L.; Lohmüller, B.; Heske, C.; Umbach, E.; Riedl, W.; Zweigart, S.; Karg, F. Flat Conduction-Band Alignment at the CdS/$CuInSe_2$ Thin-Film Solar-Cell Heterojunction. *Appl. Phys. Lett.* **2001**, *79*, 4482−4484.
(31) Bär, M.; Nishiwaki, S.; Weinhardt, L.; Pookpanratana, S.; Fuchs, O.; Blum, M.; Yang, W.; Denlinger, J. D.; Shafarman, W. N.; Heske, C. Depth-Resolved Band Gap in $Cu(In,Ga)(S,Se)_2$ Thin Films. *Appl. Phys. Lett.* **2008**, *93*, No. 244103.
(32) Jackson, P.; Hariskos, D.; Wuerz, R.; Kiowski, O.; Bauer, A.; Friedlmeier, T. M.; Powalla, M. Properties of $Cu(In,Ga)Se_2$ Solar Cells With New Record Efficiencies up to 21.7%. *Phys. Status Solidi RRL* **2015**, *9*, 28−31.
(33) Schmid, D.; Ruckh, M.; Grunwald, F.; Schock, H. W. Chalcopyrite/Defect Chalcopyrite Heterojunctions on the Basis of $CuInSe_2$. *J. Appl. Phys.* **1993**, *73*, 2902−2909.
(34) Tuttle, J. R.; Albin, D. S.; Noufi, R. Thoughts on the Microstructure of Polycrystalline Thin Film $CuInSe_2$ and Its Impact on Material and Device Performance. *Sol. Cells* **1991**, *30*, 21−38.
(35) Liao, D.; Rockett, A. Cu Depletion at the $CuInSe_2$ Surface. *Appl. Phys. Lett.* **2003**, *82*, 2829−2831.
(36) Kiss, J.; Gruhn, T.; Roma, G.; Felser, C. Theoretical Study on the Structure and Energetics of Cd Insertion and Cu Depletion of $CuIn_5Se_8$. *J. Phys. Chem. C* **2013**, *117*, 10892−10900.
(37) Ghorbani, E.; Kiss, J.; Mirhosseini, H.; Roma, G.; Schmidt, M.; Windeln, J.; Kühne, T. D.; Felser, C. Hybrid-Functional Calculations on the Incorporation of Na and K Impurities into the $CuInSe_2$ and $CuIn_5Se_8$ Solar-Cell Materials. *J. Phys. Chem. C* **2015**, *119*, 25197−25203.
(38) Lepetit, T. Influence of KF Post Deposition Treatment on the Polycrystalline $Cu(In,Ga)Se_2$/CdS Hetero-Junction Formation for Photovoltaic Application. Ph.D. Thesis, Université de Nantes, 2015.

DOI: 10.1021/acsami.8b18216
ACS Appl. Mater. Interfaces 2019, 11, 3024−3033